

DIRECT NUMERICAL SIMULATION OF FLUID FLOW AT SUPERCRITICAL PRESSURE IN A VERTICAL CHANNEL

W. Wang and S. He*

Department of Mechanical Engineering, The University of Sheffield, Sheffield, S1 3JD, UK
*s.he@sheffield.ac.uk

ABSTRACT

Fluids at a supercritical pressure are accompanied by strong variations of thermo-properties, buoyancy-influences and “abnormal” thermal developments, which have complex and interactive effects on turbulence and heat transfer, making predictions and modelling of such flows a difficult task. In order to isolate effects of variable properties and buoyancy from intricate thermal and flow developments, a vertical channel flow with constant but different wall temperatures is investigated using direct numerical simulation. The aim of this study is to understand the mechanisms of buoyancy effects on turbulence and heat transfer in water at supercritical pressure, and to provide detailed data to aid the development and validation of advanced turbulence models as well as sub-channel/system models. For the prescribed conditions, heat input from the heating wall and heat removal from the cooling wall are balanced to finally achieve a fully developed state with no heat advection but only thermal diffusion statistically. The influences of the temperature differences between the two walls are reported. Velocity, temperature, turbulence heat flux, turbulence shear stress, shear production and buoyancy production are discussed. Visualization of instantaneous flow structures is also shown.

KEYWORDS

Fully developed channel flow, turbulent heat transfer at supercritical pressure, buoyancy effects, direct numerical simulation

NOMENCLATURE	
c_p	specific heat at constant pressure
g	gravitational acceleration
Gr	The Grashof number
h	enthalpy
Nu	Nusselt number
p	pressure
P_{cri}	critical pressure
P_{uu}^{bf}, P_{uv}^{bf}	buoyancy production for $\overline{\rho u'' u''}, \overline{\rho u'' v''}$
P_{uu}^{st}, P_{uv}^{st}	shear production for $\overline{\rho u'' u''}, \overline{\rho u'' v''}$
Pr	Prandtl number
q	heat flux
Re	Reynolds number
t	time
T	temperature
T_{cri}	critical temperature
U_0	reference velocity
u_i	i th velocity vector component, $i=1,2,3$, the same as u, v, w
u, v, w	velocity vector components for the streamwise x , normal y and spanwise direction z
x_i	i th coordinate directions, $i=1,2,3$, the same as x, y, z
x, y, z	the coordinate directions in the streamwise x , normal y and spanwise direction z
+	dimensionless values scaled by wall unit
'	turbulent fluctuation with respect to Reynolds averages
''	turbulent fluctuation with respect to Favre averages
<i>Greek symbols</i>	
α	heat transfer coefficient
β	volumetric expansion coefficient
δ	half channel height
δ_{ij}	Kronecker delta
Δ	differences
λ	thermal conductivity
ρ	density
μ	Dynamic viscosity
τ_{ij}	stress tensor
$\overline{\rho u_i'' u_j''}$	Favre averaged turbulent stress
<i>Subscripts</i>	
0	reference value
b	bulk mean value
c	cold wall value
h	hot wall value
rms	root mean square value
w	wall value
<i>Superscripts</i>	
*	dimensional values
~	Favre averaged variables
-	Reynolds averaged variables

1. INTRODUCTION

The Generation IV International Forum (GIF) in 2002 chose the supercritical water-cooled reactor (SCWR) as one of six nuclear systems due to its high power conversion efficiency [1]. Since then, heat transfer characteristics to water at supercritical pressure have obtained more intensive investigation in both laboratory experiments and numerical simulations. With the development of high performance computing technology in recent decades, computational fluid dynamics (CFD) has become an affordable and powerful tool in studying fluid flow and heat transfer. Direct numerical simulation (DNS) is a new branch, which directly solves the governing equations without introducing modelling and hence produces high fidelity simulations of turbulence, flow and heat transfer. DNS is widely accepted to be able to produce data complementary to experimental data for the understanding of turbulence physics and improving simulation models. This paper reports a DNS study of turbulence and heat transfer in water at supercritical pressure in vertical parallel channel.

The thermal dynamic critical point of water is $T_{cri} = 374 \text{ }^\circ\text{C}$ (647 K) for the supercritical temperature and $P_{cri} = 22.1 \text{ MPa}$ for the supercritical pressure. **Figure 1** shows the thermal physical properties of water at 23.5 MPa, a pressure slightly above its critical value. Within a modest temperature range across the pseudo-critical temperature, thermal dynamic and thermal physical properties of water show dramatic variations. Depending on flow development and wall thermal conditions, these large variations of thermal properties can cause significant changes in heat transfer characteristics of turbulence flow, among which heat transfer deterioration (HTD) is usually undesirable. In order to improve SCWR plant safety and efficiency, fundamental research of turbulence heat transfer to supercritical water is necessary.

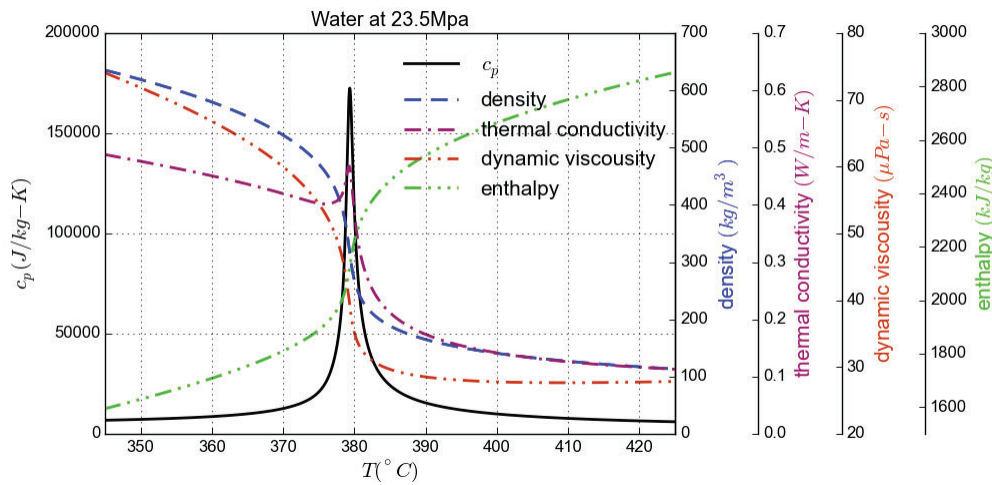


Figure 1. Thermal physical properties of water at 23.5 MPa.

Heat transfer of fluids at the supercritical pressure received relatively less attention after its initial prosperity in 1960s-1970s, but the application in reactor plants revived the interests in supercritical fluids in the recent decade. Piore et al. summarized experimental heat transfer in both supercritical water [2] and supercritical carbon dioxide [3]. As above surveys displayed, water has received less attention than carbon dioxide as the latter has a much lower critical pressure and temperature, which makes experiments much easier. Due to the lack of fluid-to-fluid scaling study, heat transfer data obtained using carbon dioxide cannot be directly used for water. Considering the application in SCWR, dedicated study of heat/flow characteristics of water at supercritical pressure is desirable. Since the review by Piore et al. [2] [3], some more study on water at supercritical pressure has emerged. Pis'menny et al. [4] preformed physical experiments for water at supercritical pressure in a vertical pipe at Reynolds number around 35000. Niceno and Sharabi [5] validated a large eddy simulation of supercritical water at the same condition but replacing the pipe with parallel plates. Numerous RANS studies of water at supercritical

water were carried out in different geometries, such as circular tubes [6-11], annulus [12-13], rectangular duct [14-15] and bundles [16-17]. DNS study of water at supercritical pressure is limited to low Reynolds numbers. Liu et al. [12] studied the influences of mass flux to HTD for supercritical water in upward annular channel using RANS, and found that HTD at low mass flux is mainly caused by buoyancy effect, while HTD at high flux is mainly due to variation of fluid properties and the acceleration effect. Considering the current computing capacity, DNS studies have to be limited to low mass flux flows. Our DNS study focuses on low mass flux and heat flux fluids, investigating buoyancy effect on turbulence statistics and heat transfer in vertical channel flow.

Fluids at supercritical pressure have strong non-uniform thermo-properties, buoyancy-influences and “abnormal” thermal developments, which may interact with each other and hence makes the understanding of individual effects on turbulence and heat transfer a difficult task. The studies with constant wall heat flux conditions (most of publications on supercritical fluids belong to this group) involves complex interaction between flow development and heat transfer characteristics. Although- these studies mimicked conditions of physical experiments and real applications to some extent, on the other hand, a simple flow setup, which decouples the various flow physics, may be advantageous in fundamental research. In 1960s, Khan [18] and McFall [19] carried out experiments on carbon dioxide flowing through both horizontal and vertical plane passages with constant but different wall temperatures. The initial motivation in designing such experiments was that under such a condition, the flow might reach a fully developed stable state with zero net heat input. The statistic temperature distribution in the streamwise direction would be constant after a sufficient distance. As a result, there would be no heat advection but only thermal diffusion. Therefore, the effects of variable properties and buoyancy would be separated from the intricate effects of the thermal/flow development. However, these conditions were quite difficult to be achieved in real experiments. For example, heat radiation always exists between the two walls. In addition, the strong influences of buoyancy also led to ill-defined and non-uniform thermal wall temperatures, as commented by Jackson [20]. With the development of high performance computing, numerical study of supercritical fluids makes the above flow configuration feasible.

To achieve the aim of understanding thermal physics in a fully developed flow, a series of numerical experiments have been performed to study the influences on heat transfer characteristics. In our study, the cooling wall temperature is fixed, and the heating wall temperature increases gradually from under pseudo-critical temperature to above it in a series of cases. In this paper, results of upward flow with two different heating wall temperatures are reported.

2. GOVERNING EQUATIONS

In a supercritical water-cooled reactor, the flow can be considered incompressible and the acoustic interactions and compressibility effects are negligible. The thermal properties may vary significantly with temperature but can be assumed to be independent of the pressure variation. In the equation of energy conservation, heat from viscous dissipation and work done by gravity are also neglected because they are much small in comparison with other terms. Based on all these assumptions, an in-house direct numerical simulation code has been developed to study heat transfer to fluids at supercritical pressures.

The governing equations in dimensionless form, including the mass conservation equation, the momentum conservation equation and the energy conservation equation, are shown below,

$$\frac{\partial \rho}{\partial t} + \frac{\partial \rho u_i}{\partial x_i} = 0 \quad (1)$$

$$\frac{\partial \rho u_i}{\partial t} + \frac{\partial \rho u_i u_j}{\partial x_j} = -\frac{\partial p}{\partial x_i} + \frac{1}{Re_0} \cdot \frac{\partial \tau_{ij}}{\partial x_j} - \frac{\delta}{U_0^2} \rho g \cdot \delta_{1i} \quad (2)$$

$$\frac{\partial \rho h}{\partial t} + \frac{\partial \rho h u_j}{\partial x_j} = \frac{1}{Re_0 Pr_0} \cdot \frac{\partial}{\partial x_j} \left(\lambda \frac{\partial T}{\partial x_j} \right) \quad (3)$$

The definitions of dimensionless variables are

$$t = \frac{t^*}{\delta/U_0}, x_i = \frac{x_i^*}{\delta}, u_i = \frac{u_i^*}{U_0}, p = \frac{p^*}{\rho_0 U_0^2}, \phi = \frac{\phi^*}{\phi_0} \quad (\phi = T, \rho, \mu, \lambda, c_p), h = \frac{h^* - h_0}{c_{p0} T_0}, Re_0 = \frac{\rho_0 U_0 \delta}{\mu_0}, Pr_0 = \frac{\mu_0 c_{p0}}{\lambda \kappa_0} \quad (4)$$

where the superscript * stand for dimensional quantities. All the flow and thermal variables are normalized by properties at a reference state with the subscript 0. The negative sign of the gravity term stands for that the direction of the gravity force is opposite to the positive coordinate direction.

Above equations are solved on a staggered mesh with a second order central difference finite-difference method. A pressure-correction method for the incompressible flow is implemented to enforce the continuity equation. For the temporal discretization, a third order explicit Runge-Kutta scheme is used for the nonlinear terms, and a second order implicit Crank-Nicholson scheme for the linear terms in the momentum equations. Details on the spatial discretization schemes for the momentum and continuity equations were given in [22]. For the energy equation, enthalpy is calculated using an explicit Runge-Kutta method. The process to solve the coupled governing equations in each Runge-Kutta stage is as follows: firstly, the energy equation is solved to obtain a provisional enthalpy; then, temperature, density, viscosity and thermal conductivity are updated based on this enthalpy. This is done by searching a physical property table generated with the NIST 9.1 database [23]; then, based on the updated temperature, a new enthalpy is searched; next, the momentum equations are solved with updated density and viscosity; finally, the continuity equation is satisfied by a predictor-corrector method via solving the Poisson equation. The solving procedure is similar to [24].

3. COMPUTATIONAL CONFIGURATION

3.1. Geometry and Mesh

DNS was carried out for water at a pressure of 23.5 MPa in a channel with the height of $2\delta = 3$ mm. The Reynolds number based on the half channel height is $Re_0 = 2800$ for the isothermal flow. We consider a flow in a vertical parallel channel with the temperatures of its two walls fixed at constant but different values. A sketch of the vertical channel flow is shown in **Figure 2**. When the flow reaches developed state, the heat input from the hotter wall (the right hand side in **Figure 2**) will be balanced by the heat removal from the colder wall (on the left hand side) and hence there is no advection of heat in the streamwise direction. Considering these features, a periodic boundary condition is applied in streamwise and spanwise directions of the computational domain. The computational domain for the channel flow is 16δ , 4δ and 2δ in the streamwise, spanwise and wall-normal directions, respectively. The numbers of grid points in these three directions are 512, 160 and 160, and the corresponding grid resolutions in wall unit for the isothermal flow are $\Delta x^+ \approx 5.6$, $\Delta z^+ \approx 4.5$ and $0.4 < \Delta y^+ < 4.4$. **Figure 3** shows the mean velocity and turbulence intensity for the isothermal flow, comparing with the DNS data of [25] marked as “MKM180”. Both the mean velocity and the turbulence intensity in all the three directions show good agreements with the reference data, and both display symmetric distribution along the channel centre.

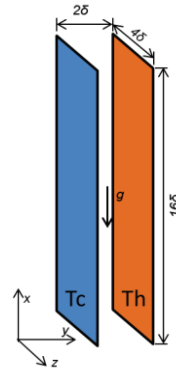


Figure 2. Sketch of the vertical channel flow.

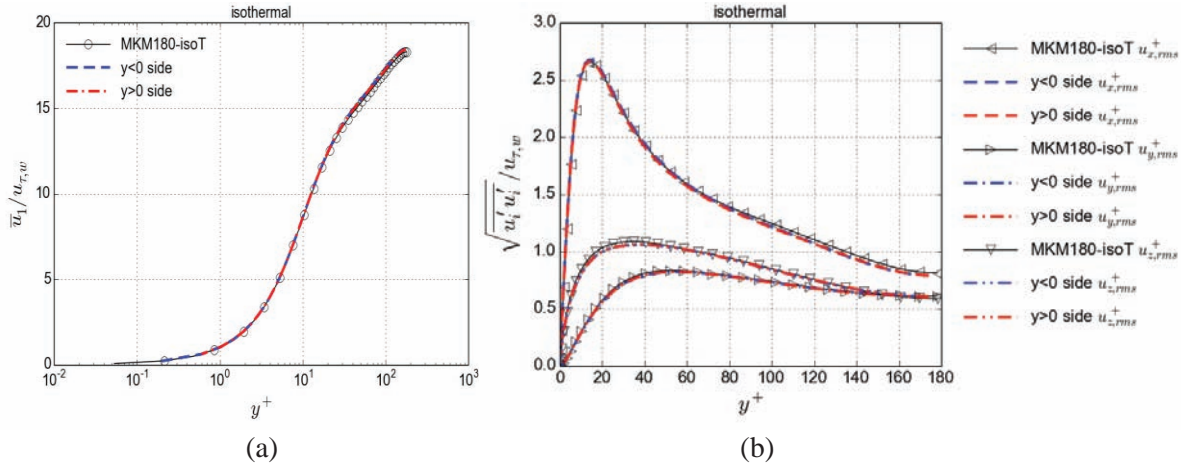


Figure 3. Isothermal flow (a) the mean velocity, (b) root mean square of velocities

3.2. Initial and boundary conditions

Temperature $T_0 = 372^\circ\text{C}$ (645.15 K) is chosen as reference temperature, and dimensionless variables are scaled based on the absolute values of parameters at this temperature. In the current study, the mass flux is $108.6 \text{ kg/m}^2\text{s}$, which is kept the same for all cases. A summary of the wall temperatures for the studied cases is given in **Table I**. Group-1 has a heating wall temperature below the pseudo-critical temperature, and group-2 has a heating wall temperature above it. In each group, both the forced convection and upward mixed convection flow are studied. In forced convection, gravity is omitted, and these cases study the effects of variable properties. As for the mixed convection cases, both the gravity and variable properties are fully considered in the governing equations. Based on the current coordinate system, the cooling wall locates at $y/\delta = -1$, and the heating wall at $y/\delta = +1$, and the gravity direction coincides with the negative x-direction. The no-slip boundary condition is applied on the two channel walls.

Table I. Cases and their wall temperature setting-up

Case	isothermal	Group-1		Group-2	
		Forced-1	Upward-1	Forced-2	Upward-2
T_c (unit: $^\circ\text{C}$)	372.0	367.0	367.0	367.0	367.0
T_h (unit: $^\circ\text{C}$)	372.0	377.0	377.0	380.0	380.0
ΔT (unit: $^\circ\text{C}$)	0	10	10	13	13

4. RESULTS AND DISCUSSIONS

Both the Reynolds averaged and the Favre averaged variables are used to present results. The Reynolds average is defined as an average over both time and the homogenous directions (the streamwise and spanwise directions), labelled as $\bar{\varphi}$, where φ is any variable. The Favre average is defined as $\tilde{\varphi} = \bar{\rho\varphi}/\bar{\rho}$. The relations between the averaged mean and fluctuations in these two averaging schemes are

$$\varphi' = \varphi - \bar{\varphi} \tag{5}$$

$$\varphi'' = \varphi - \tilde{\varphi} \tag{6}$$

4.1. Bulk Parameters

Table II summarizes the bulk and wall parameters. The symbol α stands for heat transfer coefficient, defined as

$$\alpha = q_w / (T_w - T_b) \quad (7)$$

The Grashof number in this study is defined based on the temperature differences between two walls rather than the density differences used in [21], and the expression is

$$Gr = g\beta\rho^2(T_h - T_c) \cdot (2\delta)^3 / \mu^2 \quad (8)$$

The Nusselt number is defined as

$$Nu = 2\delta / \lambda_b \cdot q_w / (T_w - T_b) \equiv 2\delta / \lambda_b \cdot \alpha \quad (9)$$

Simulation results show that the bulk temperatures T_b in both groups are below the pseudo-critical temperature in the current setup and the wall-normal direction locations for $T = T_b$ for all studied cases are biased towards the heating wall except for “forced-1”, which locates at almost the centre of the channel. Heat flux q_w is the energy input through the heating wall into the system and removal from the system through the cooling wall, which two are balanced at the fully developed state, and it is much smaller (15.78~44.1 kW/m²) than those in the widely studied constant wall heat flux conditions (usually >100 kW/m² [2]). Increasing the heating wall temperature from 377.0 °C (group-1) to 380.0 °C (group-2), the wall heat flux for “upward-2” is more than doubled compared to “upward-1”, while “forced-2” has a slightly smaller heat flux than “forced-1”. The heat transfer coefficient is plotted against the wall temperature in **Figure 4** (a). Similar to the wall heat flux, the heat transfer coefficient α in “forced-2” is smaller than that in “forced-1”, while “upward-2” has a higher heat transfer coefficient than “upward-1”. In comparison with forced convection flow, heat transfer coefficient is increased on both walls in the mixed convection, due to enhancement of turbulent diffusion of heat. Besides, in both the forced and the upward cases, increased heating wall temperature results in an enhanced heat transfer in the heating wall side. **Figure 4** (b) compares the Nusselt number ratio in the current DNS of water with the correlation formulas used in [21] for carbon dioxide. The normalized Nusselt numbers in the heating wall in both groups agree well with the given correlation plots. Heat transfer characteristics for the upward cooling side are equivalent to downward heating flow. Thus, it is expected that the “upward-1” cooling side has normalized Nusselt number located around the line of the downward heating correlation plot. However, the cooling side in “upward-2” has a much larger normalized Nusselt number. An important reason is that the buoyancy effect assessed using the bulk temperature is not representative of the real buoyancy since the properties around the pseudo-critical temperature vary rapidly which is not reflected in the buoyancy parameter.

Table II. Summary of bulk and wall parameters

Case	Group1		Group2	
	Forced-1	Upward-1	Forced-2	Upward-2
T_b (°C)	373.3	372.7	378.0	376.2
q_w (kW/m ²)	17.2	21.1	16.4	41.7
y/δ for $T = T_b$	-0.01	0.21	0.12	0.41
Re_b	5730	5670	6828	6188
Pr_b	2.2	2.1	6.3	3.4
$Gr_b/Re_b^{2.7} \times 10^4$	-	2.9	-	6.0
Nu_c	20.0	26.7	10.4	33.1
Nu_h	32.9	35.2	58.6	78.7
α_c (kW/(m ² K))	2.8	3.7	1.5	4.6
α_h (kW/(m ² K))	4.6	4.9	8.4	10.8
$\tau_{w,c} \times 10^{-3}$ (kg/(ms ²))	3.6	3.1	2.3	2.6
$\tau_{w,h} \times 10^{-3}$ (kg/(ms ²))	5.0	7.1	8.2	12.3

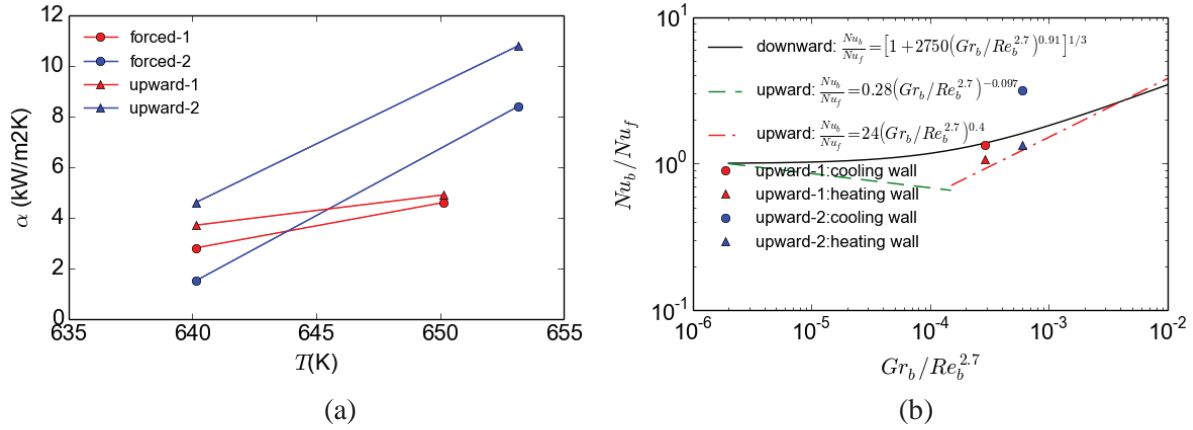


Figure 4 (a) Heat transfer coefficient on both cooling and heating walls. (b) Comparison of the Nusselt number ratio between the current DNS of water and correlations used in [21] for CO₂.

4.2. Turbulence Statistics and Buoyancy Production

The influence of buoyancy on the mean flow profile and on the production of turbulence will be studied to reveal heat transfer behavior of turbulent mixed convection in a vertical flow. The expression of the shear production for the fully developed flow is degraded, compared with its original expression. The

shear productions P_{uu}^{st} for $\overline{\rho u_1'' u_1''}$ is

$$P_{uu}^{st} = -2 \left(\overline{\rho u_1'' u_1'' \frac{\partial \bar{u}_1}{\partial x}} + \overline{\rho u_1'' u_2'' \frac{\partial \bar{u}_1}{\partial y}} + \overline{\rho u_1'' u_3'' \frac{\partial \bar{u}_1}{\partial z}} \right) = -2 \overline{\rho u_1'' u_2'' \frac{\partial \bar{u}_1}{\partial y}} \quad (10)$$

The shear productions P_{uv}^{st} for $\overline{\rho u_1'' u_2''}$ is

$$P_{uv}^{st} = - \left(\overline{\rho u_1'' u_1'' \frac{\partial \bar{u}_2}{\partial x}} + \overline{\rho u_1'' u_2'' \frac{\partial \bar{u}_2}{\partial y}} + \overline{\rho u_1'' u_3'' \frac{\partial \bar{u}_2}{\partial z}} \right) - \left(\overline{\rho u_2'' u_1'' \frac{\partial \bar{u}_1}{\partial x}} + \overline{\rho u_2'' u_2'' \frac{\partial \bar{u}_1}{\partial y}} + \overline{\rho u_2'' u_3'' \frac{\partial \bar{u}_1}{\partial z}} \right) = - \overline{\rho u_2'' u_2'' \frac{\partial \bar{u}_1}{\partial y}} \quad (11)$$

For an upward flow with gravity force opposite to the flow direction, the buoyancy production P_{uu}^{bf} for $\overline{\rho u_1'' u_1''}$ is

$$P_{uu}^{bf} = -2g\delta/U_0^2 \overline{\rho' u_1'} \quad (12)$$

And, the buoyancy production P_{uv}^{bf} for $\overline{\rho u_1'' u_2''}$ is

$$P_{uv}^{bf} = -g\delta/U_0^2 \overline{\rho' u_2'} \quad (13)$$

Figure 5(a) and **(b)** show the shear and buoyancy production of the turbulent shear stress $\overline{\rho u_1'' u_2''}$. Overall, the buoyancy production is far less than the shear production, as expected in the upward flow where the buoyancy production plays a secondary role. **Figure 5(b)** shows that the buoyancy production for the shear stress in the upward flow is a sink of turbulence and increased heating wall temperature aggravates the sinking. As Eq. (11) shown, the distribution of the shear production of $\overline{\rho u_1'' u_2''}$ purely depends on the Reynolds normal stress $\overline{\rho u_2'' u_2''}$ (shown in **Figure 5(c)**) and the gradient of the mean velocity. There is neither stress production nor buoyancy production for $\overline{\rho u_2'' u_2''}$ for fully developed channel vertical flow, while the pressure strain dominates its distribution. **Figure 5(a)** and **(c)** show that compared to the isothermal flow, two forced convection flow has reduced $\overline{\rho u_2'' u_2''}$ near the cooling wall side, where the stress production is also reduced. Nevertheless, $\overline{\rho u_2'' u_2''}$ is increased near the heating wall side, correspondingly, the stress production rises. It can be seen from **Figure 5(a)** and **(c)** that the higher heating wall temperature intensifies the reduction in the stress production near the cooling wall and the increase near the heating wall. Besides, the distribution of the shear stress (**Figure 5(d)**) for the forced convection is asymmetric, due to the effects of variable properties. For the mixed convection flow,

$\overline{\rho u_2'' u_2''}$ has stronger increase near the cooling wall, and then it decreases towards the heating wall, where there is another rapid increase before falling to zero on the wall. Near the heating wall side, the difference in heating wall temperature between “group-1” and “group-2” introduces stronger variations of $\overline{\rho u_2'' u_2''}$ than the buoyancy effect in the same group. Correspondingly, the distribution of the stress production (Figure 5(a)) also follows similar trends. The positive contribution of the stress production near both walls results in higher shear stress. Another significant influence of buoyancy on the flow is that it distorts the total shear stress which is a linear distribution in both the isothermal and forced flow. This is resulted from the non-uniform distribution of the buoyancy force due the variation of the fluid temperature.

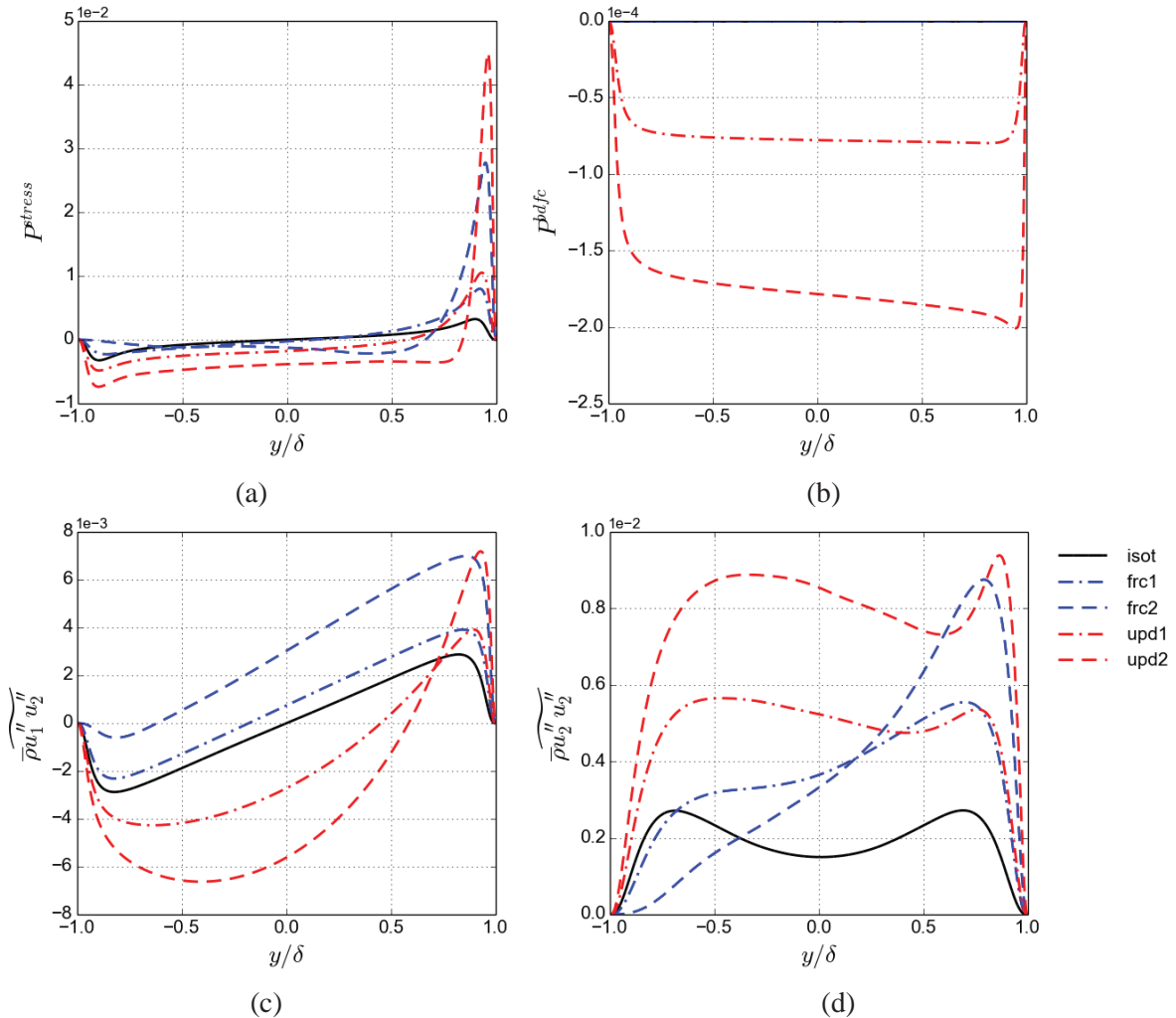


Figure 5 (a) The stress production for $\overline{\rho u_1'' u_2''}$. (b) The buoyancy production for $\overline{\rho u_1'' u_2''}$. (c) the turbulence normal stress $\overline{\rho u_2'' u_2''}$ (d) the turbulence shear stress $\overline{\rho u_1'' u_2''}$

Figure 6 (a) and (b) show the stress and buoyancy production for the streamwise normal stress $\overline{\rho u_1'' u_1''}$. Again, the buoyancy production is much smaller than the stress production. **Figure 6** (b) shows that the buoyancy production for the normal stress $\overline{\rho u_1'' u_1''}$ is positive across the flow except for regions close to the heating wall in both upward flows. In “upward-2”, there are two peaks in positive buoyancy production near two walls, while in the “upward-1” with a lower T_h , there is a larger region where contribution of buoyancy production near the heating wall is negative. **Figure 6** (b) and (c) displays that

near the cooling wall side, the stress production for “forced-2” strongly reduces, and so does the streamwise normal stress $\overline{\rho u_1'' u_1''}$. While, near the heating wall, all cases has increased stress production, especially for “group-2” with a higher wall temperature.

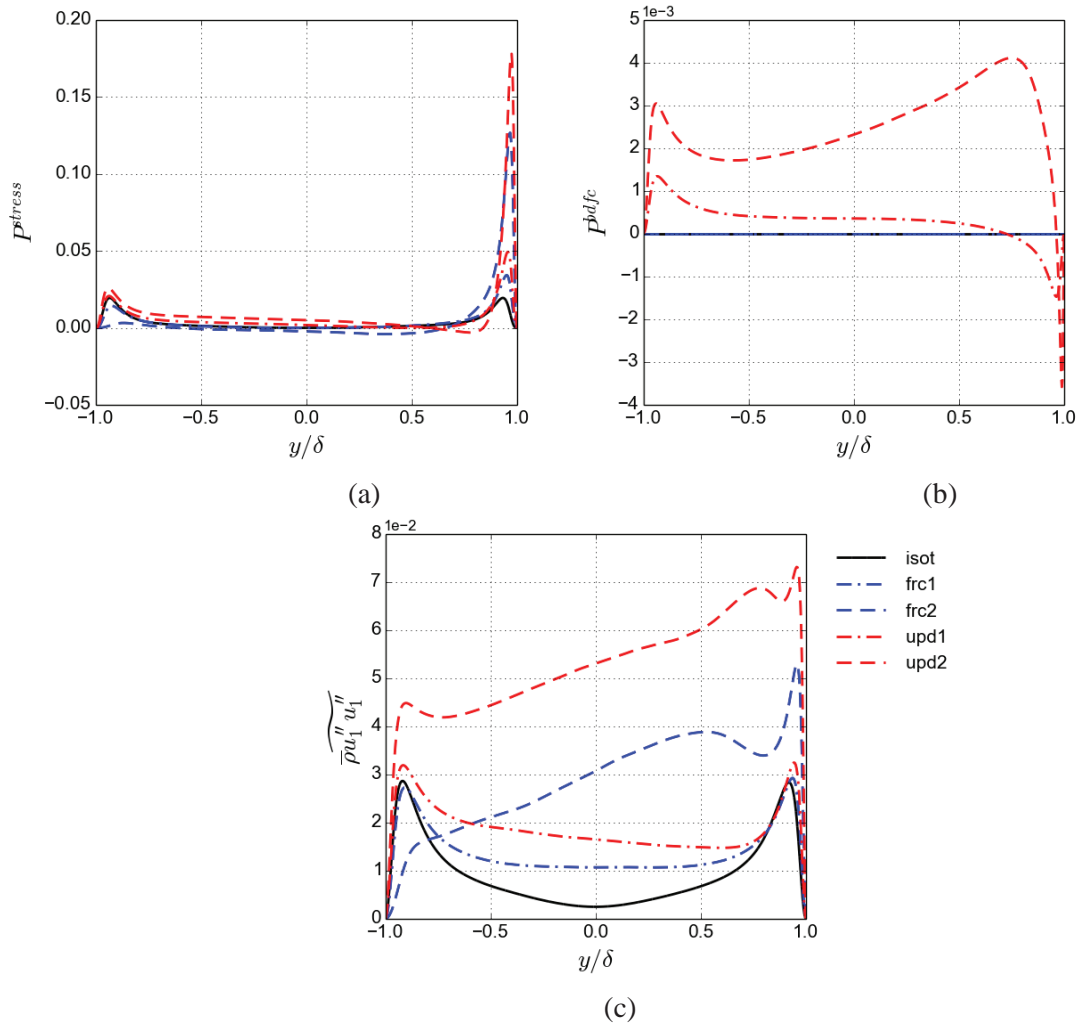


Figure 6 (a) The stress production for the streamwise normal stress $\overline{\rho u_1'' u_1''}$. (b) The buoyancy production for streamwise normal stress $\overline{\rho u_1'' u_1''}$. (c) the streamwise normal stress $\overline{\rho u_1'' u_1''}$.

Figure 7 (a) shows the distribution of Favre averaged streamwise velocity profile. The distribution of velocity is a result of complicated effects of buoyancy force and variable properties. “Forced-1” and “forced-2” both have slight deficit of velocity near the cooling wall ($-1 < y/\delta < -0.7$), and the deficit in “force-2” is more severe. Then, towards the heating wall, the velocity increases rapidly for “forced-2”. The dramatic increase of the velocity near the wall is related with the severe reduction of the viscosity (shown in **Figure 7 (a)**).
Figure 7 (b). The two upward cases has similar velocity trends near the cooling wall, and in $y/\delta > -0.2$, the “upward-2” increases more quickly than “upward-1” due to both the smaller molecular viscosity and stronger buoyancy influences.

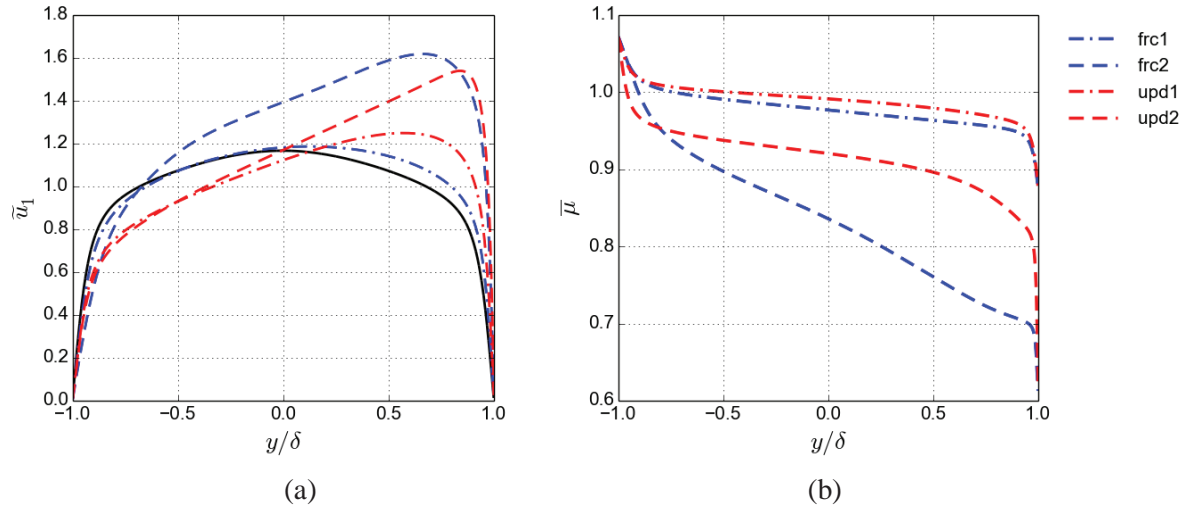


Figure 7 (a) Favre averaged streamwise velocity distribution, (b) the molecular viscosity

4.3. Turbulent Heat Flux and Property Asymmetry

Figure 8 (a) displays the distribution of the streamwise turbulent heat flux $\overline{\rho u_1'' h''}$ and **Figure 8 (b)** shows the wall-normal turbulent heat flux $\overline{\rho u_2'' h''}$. It is observed that both the forced and upward flow in group-2 has two positive peaks of turbulence heat flux $\overline{\rho u_1'' h''}$, while the group-1 only has one positive peak near the cooling wall and then it gradually decreases towards the heating wall and reaches a negative peak near the heating wall. This implies that the temperature of the heating wall, rather than the buoyancy force in this study, plays a dominant role in the streamwise turbulent heat flux distribution. For the upward flow, the distribution of the streamwise turbulent heat flux $\overline{\rho u_1'' h''}$ is similar to $-2g\delta/U_0^2 \overline{\rho' u_1'}$. The reason is that $\overline{u_1' h'}$, the main contribution of $\overline{\rho u_1'' h''}$, has the same trend as $\overline{\rho' u_x'}$, due to the monotonic dependence of density on enthalpy. The wall-normal turbulent heat flux $\overline{\rho u_2'' h''}$ is one order of magnitude smaller than $\overline{\rho u_1'' h''}$, but plays a more important role, as it directly related heat transfer between heating and cooling walls. The distribution of $\overline{\rho u_2'' h''}$ is largely related to the shear stress distribution, as the latter represents the turbulence diffusion of the heat. The upward flow has a much larger $-\overline{\rho u_2'' h''}$ than the forced flow, and the buoyancy effect in group-2 with higher heating wall temperature is stronger. The influence of buoyancy and the wall temperature both significantly influence these distributions.

Figure 9 displays the wall-normal distributions of enthalpy, temperature and density. Comparing two forced convection cases, because of the decreased turbulence diffusion of heat near the cooling wall in “forced-2”, the thermal boundary layer is thicker in this case than in “forced-1”. The heat transfer deterioration near the cooling wall in “forced-2” also results in a higher T_b and larger temperature distribution and smaller density due to gas-like state. Within each group with the same wall temperatures, the upward flow has a flatter distribution of temperature, due to a stonger turbulent heat diffusion.

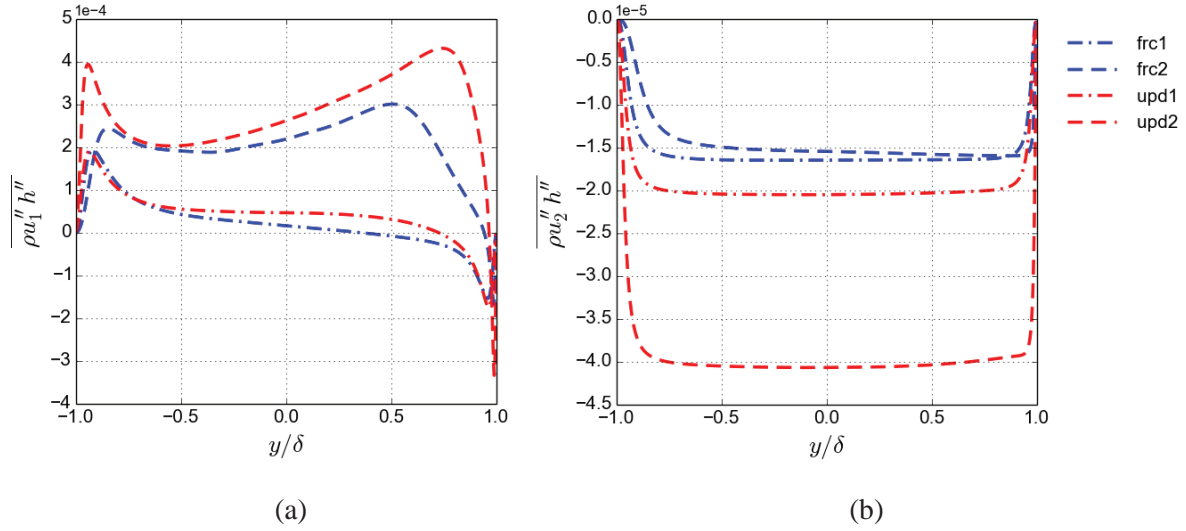


Figure 8. (a) Streamwise turbulent heat flux distribution $\overline{\rho u_1'' h''}$, (b) wall-normal turbulent heat flux distribution $\overline{\rho u_2'' h''}$

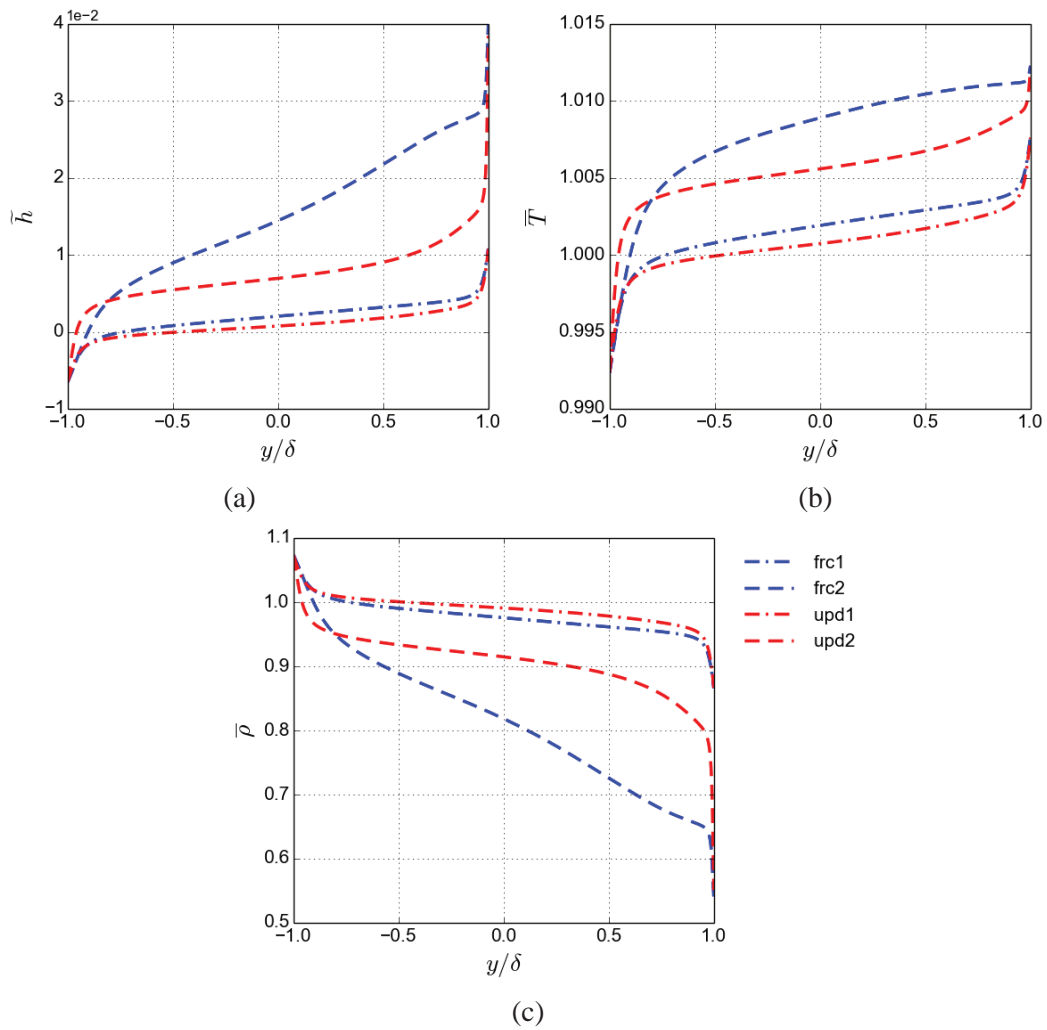


Figure 9 (a) Farve averaged enthalpy, (b) Temperature distribution, (c) Density distribution

4.4. Instantaneous Flow Structures

The instantaneous flow structures are shown to visualize the buoyancy effect on turbulent flow structures. Figure 10 displays the instantaneous flow structures with the λ_2 criterion [26]. Here, λ_2 is the second largest eigenvalue of the symmetric tensor $\mathbf{S}^2 + \mathbf{\Omega}^2$ where \mathbf{S} and $\mathbf{\Omega}$ are the symmetric and antisymmetric parts of the velocity gradient tensor $\nabla \mathbf{u}$. For the forced convection, turbulence is damped near the cooling wall, and is enhanced near the heating wall. “Forced-2” with a higher T_h has less turbulence fluctuations near the cooling wall and more near the heating wall. For the upward flow, turbulence enhancement is observed both near the cooling wall and heating wall and the increase in the heating wall temperature further increases turbulence.

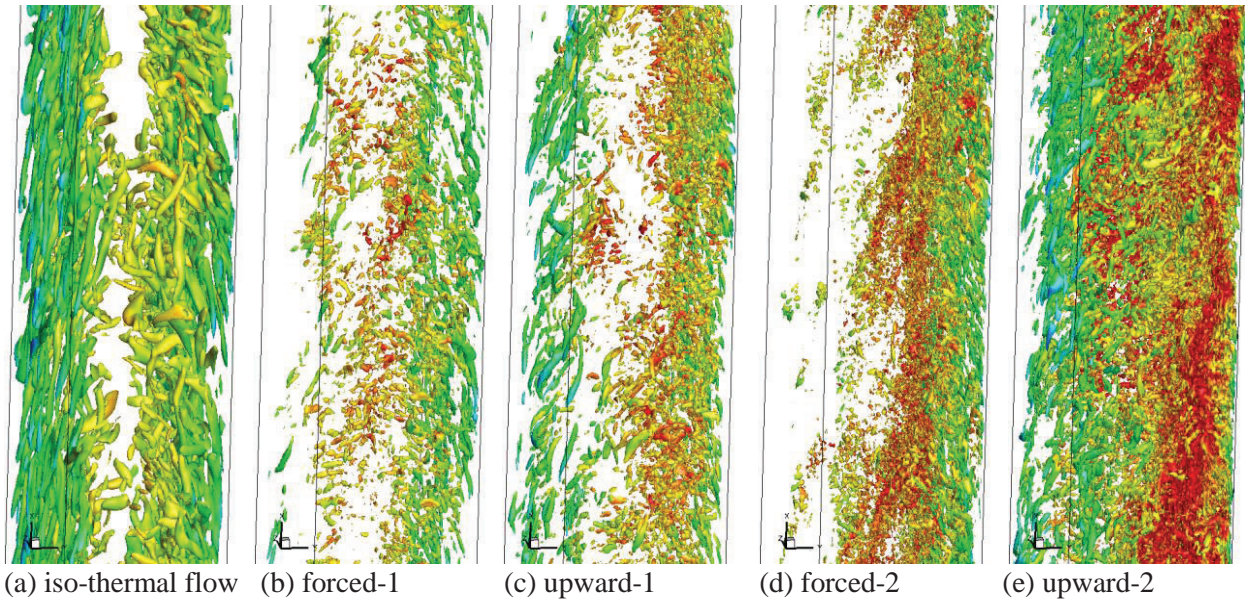


Figure 10 Instantaneous iso-surface of λ_2 criterion, coloured by the streamwise velocity. The left surface is cooling wall and the right surface is the heating wall. For the isothermal flow, $\lambda_2 = -1$, and $\lambda_2 = -10$ for all others.

5. CONCLUSIONS

This study investigates the characteristics of turbulent heat transfer to water at a supercritical pressure in an upward channel with constant but different wall temperatures using direct numerical simulation. Turbulence statistics, buoyancy effects and heat transfer are discussed.

The turbulent shear stress is suppressed near the cooling wall and enhanced near the heating wall in the forced convection cases. Increasing the heating wall temperature intensifies this effect. Such effect on turbulence can also be seen from the heat transfer rate. Heat transfer is deteriorated near the cooling wall and enhanced near the heating wall. For the mixed convection flows, the turbulent shear stress is increased overall, especially near the heating wall and the central region of the channel. With the increase of the temperature of the heating wall, turbulence is further increased, so is turbulent heat flux.

ACKNOWLEDGMENTS

This work is supported by the Engineering and Physical Sciences Research Council of the United Kingdom under Grant No. EP/K007777/1. This work made use of the facilities of the N8 HPC, provided

and funded by the N8 consortium and EPSRC (Grant No. EP/K000225/1). The Centre is co-ordinated by the Universities of Leeds and Manchester.

REFERENCES

1. DoE, U. S. "A technology roadmap for generation IV nuclear energy systems." *Nuclear Energy Research Advisory Committee and the Generation IV International Forum*. (2002).
2. Pioro, I. L., and Duffey, R.B. "Experimental heat transfer in supercritical water flowing inside channels (survey)." *Nuclear Engineering and Design*, **235**,22, pp. 2407-2430 (2005).
3. Duffey, R.B., and Pioro, I L. "Experimental heat transfer of supercritical carbon dioxide flowing inside channels (survey)." *Nuclear Engineering and Design*, **235**,8, pp. 913-924 (2005).
4. Pis'menny, E. N., Razumovskiy, V. G., Maevskiy, E. M., Koloskov, A. E. and Pioro, I. L., "Heat Transfer to Supercritical Water in Gaseous State or Affected by Mixed Convection in Vertical Tubes", *Proceedings of ICONE14*, Miami, Florida, USA, (2006)
5. Ničeno, B., and M. Sharabi. "Large eddy simulation of turbulent heat transfer at supercritical pressures." *Nuclear Engineering and Design*, **261**, pp. 44-55 (2013).
6. Koshizuka, S., Takano, N., and Oka, Y. "Numerical analysis of deterioration phenomena in heat transfer to supercritical water". *International Journal of Heat and Mass*, **38**(16), pp. 1–8 (1995).
7. Lei, X., Li, H., Yu, S., and Chen, T. "Numerical investigation on the mixed convection and heat transfer of supercritical water in horizontal tubes in the large specific heat region". *Computers and Fluids*, **64**, pp. 127–140 (2012).
8. Zhang, G., Zhang, H., Gu, H., Yang, Y., and Cheng, X. "Experimental and numerical investigation of turbulent convective heat transfer deterioration of supercritical water in vertical tube." *Nuclear Engineering and Design*, **248**, pp. 226–237 (2012).
9. Kao, M.-T., Lee, M., Ferng, Y.-M., and Chieng, C.-C. "Heat transfer deterioration in a supercritical water channel". *Nuclear Engineering and Design*, **240**(10), pp. 3321–3328 (2010).
10. Jaromin, M., and Anglart, H. "A numerical study of heat transfer to supercritical water flowing upward in vertical tubes under normal and deteriorated conditions". *Nuclear Engineering and Design*, **264**, pp.61–70 (2013).
11. Bazargan, M., and Mohseni, M. "The significance of the buffer zone of boundary layer on convective heat transfer to a vertical turbulent flow of a supercritical fluid". *The Journal of Supercritical Fluids*, **51**(2), pp. 221–229 (2009).
12. Liu, L., Xiao, Z., Yan, X., Zeng, X., and Huang, Y. "Numerical simulation of heat transfer deterioration phenomenon to supercritical water in annular channel." *Annals of Nuclear Energy*, **53**, pp. 170-181 (2013):.
13. Zaim, E. H., and Nassab, S.A.G. "Numerical investigation of laminar forced convection of water upwards in a narrow annulus at supercritical pressure." *Energy*, **35**(10), pp. 4172–4177 (2010)
14. Lee, S. H. "Numerical study of convective heat transfer to supercritical water in rectangular ducts". *International Communications in Heat and Mass Transfer*, **37**(10), pp. 1465–1470 (2010).
15. Askari, I.B., Nassab, S.A.G. and Peymanfard, M.. "Numerical Analysis of Convective Heat Transfer in Supercritical Water Flow Channels". *Engineering Applications of Computational Fluid Mechanics*, **3**(3), pp. 408–418 (2014)
16. Cheng, X., Kuang, B., and Yang, Y. H. "Numerical analysis of heat transfer in supercritical water cooled flow channels". *Nuclear Engineering and Design*, **237**(3), pp. 240–252 (2007).
17. Yang, Z., Bi, Q., Wang, H., Wu, G., and Hu, R. "Experiment of Heat Transfer to Supercritical Water Flowing in Vertical Annular Channels". *Journal of Heat Transfer*, **135**(4), pp.042–504 (2013).
18. Khan, S. A. "Heat transfer to carbon dioxide at supercritical pressure". *Ph.D. Thesis*. University of Manchester, (1965).
19. McFall, A. "An investigation of combined forced and free convection heat transfer to supercritical pressure CO₂". *Ph.D. Thesis*. University of Manchester, (1969).

20. Jackson, J. D. "Fluid flow and convective heat transfer to fluids at supercritical pressure." *Nuclear Engineering and Design*, **264**, pp. 24-40 (2013).
21. Bae, J.H., Yoo, J.Y., and Choi, H. "Direct numerical simulation of turbulent supercritical flows with heat transfer." *Physics of Fluids*, **17.10**, pp. 105104 (2005).
22. He, S., and Seddighi, M. "Turbulence in transient channel flow." *Journal of Fluid Mechanics*, **715**, pp. 60-102 (2013).
23. Manion, J. A., Huie, R. E., Levin, R. D., Burgess, D. R., Orkin, V. L., Tsang, W., McGivern, W. S., Hudgens, J. W., Knyazev, V. D., Atkinson, D. B., Chai, E., Tereza, A. M., Lin, C.-Y., Allison, T. C., Mallard, W. G., Westley, F., Herron, J. T., Hampson, R. F., and Frizzell, D. H. "NIST Chemical Kinetics Database, NIST Standard Reference Database 17, Version 7.0 (Web Version), Release 1.6.8, Data version 2013.03", *National Institute of Standards and Technology*, Gaithersburg, Maryland, 20899-8320.
24. Pierce, C.D. and Moin, P. "Progress-variable approach for large-eddy simulation of non-premixed turbulent combustion." *Journal of Fluid Mechanics*, **504**:73-97(2004).
25. Kim, J., Moin, P. and Moser, R. "Turbulence statistics in fully developed channel flow at low Reynolds number." *Journal of fluid mechanics*, **177**, pp. 133-166 (1987).
26. Jeong, J., and Hussain, F. "On the identification of a vortex." *Journal of fluid mechanics*, **285**, pp. 69-94 (1995).